

High efficiency optical modulation at a telecom wavelength using the quantum Zeno effect in a ladder transition in Rb atoms

Subramanian Krishnamurthy,¹ Y. Wang,¹ Y. Tu,¹ S. Tseng,¹ and M. S. Shahriar^{1,2,*}

¹Department of EECS, Northwestern University, Evanston, Illinois 60208, USA

²Department of Physics and Astronomy, Northwestern University, Evanston, Illinois 60208, USA

*shahriar@northwestern.edu

Abstract: We demonstrate a high-efficiency optical modulator at ~ 1323 nm using the quantum Zeno effect in a ladder transition in a Rb vapor cell. The lower leg of the transitions represents the control beam while the upper leg of the transitions represents the signal beam. The cross-modulation of the signal beam transmission is observed as the control beam is intensity modulated, and is explained in terms of the quantum Zeno effect. We observe a modulation depth of near 100% at frequencies up to 1MHz and demonstrate modulation at speeds up to 75 MHz, with a 3 dB bandwidth of about 5 MHz, limited by the homogeneous linewidth of the intermediate state. We also describe how much higher modulation speeds could be realized by using a buffer gas to broaden the transitions. We identify and explain the special conditions needed for optimizing the modulation efficiency. Numerical simulations of modulation at ~ 1 GHz are presented. The maximum modulation speed is found to scale with the pressure-broadened linewidth of the intermediate state, so that much higher speeds should be attainable.

© 2012 Optical Society of America

OCIS codes: (020.4180) Multiphoton processes; (250.4110) Modulators.

References

1. S. E. Harris and Y. Yamamoto, "Photon switching by quantum interference," *Phys. Rev. Lett.* **81**(17), 3611–3614 (1998).
2. R. G. Beausoleil, W. J. Munro, D. A. Rodrigues, and T. P. Spiller, "Applications of electromagnetically induced transparency to quantum information processing," *J. Mod. Opt.* **51**(16-18), 2441–2448 (2004).
3. A. M. C. Dawes, L. Illing, S. M. Clark, and D. J. Gauthier, "All-optical switching in Rubidium vapor," *Science* **308**(5722), 672–674 (2005).
4. M. Bajcsy, S. Hofferberth, V. Balic, T. Peyronel, M. Hafezi, A. S. Zibrov, V. Vuletic, and M. D. Lukin, "Efficient All-optical switching using slow light within a hollow Fiber," *Phys. Rev. Lett.* **102**(20), 203902 (2009).
5. V. Venkataraman, P. Londero, A. R. Bhagwat, A. D. Slepikov, and A. L. Gaeta, "All-optical modulation of four-wave mixing in an Rb-filled photonic bandgap fiber," *Opt. Lett.* **35**(13), 2287–2289 (2010).
6. K. Salit, M. Salit, S. Krishnamurthy, Y. Wang, P. Kumar, and M. S. Shahriar, "Ultra-low power, Zeno effect based optical modulation in a degenerate V-system with a tapered nano fiber in atomic vapor," *Opt. Express* **19**(23), 22874–22881 (2011).
7. S. M. Spillane, G. S. Pati, K. Salit, M. Hall, P. Kumar, R. G. Beausoleil, and M. S. Shahriar, "Observation of nonlinear optical interactions of ultralow levels of light in a tapered optical nanofiber embedded in a hot Rubidium vapor," *Phys. Rev. Lett.* **100**(23), 233602 (2008).
8. G. Brambilla, V. Finazzi, and D. J. Richardson, "Ultra-low-loss optical fiber nanotapers," *Opt. Express* **12**(10), 2258–2263 (2004).
9. S. M. Hendrickson, M. M. Lai, T. B. Pittman, and J. D. Franson, "Observation of two-photon absorption at low power levels using tapered optical fibers in Rubidium vapor," *Phys. Rev. Lett.* **105**(17), 173602 (2010).
10. T. A. Birks, W. J. Wadsworth, and P. St. J. Russell, "Supercontinuum generation in tapered fibers," *Opt. Lett.* **25**(19), 1415–1417 (2000).

11. S. M. Spillane, T. J. Kippenberg, O. J. Painter, and K. J. Vahala, "Ideality in a fiber-taper-coupled microresonator system for application to cavity quantum electrodynamics," *Phys. Rev. Lett.* **91**(4), 043902 (2003).
12. D. J. Alton, N. P. Stern, T. Aoki, H. Lee, E. Ostby, K. J. Vahala, and H. J. Kimble, "Strong interactions of single atoms and photons near a dielectric boundary," *Nat. Phys.* **7**(2), 159–165 (2011).
13. T. Allsop, F. Floreani, K. P. Jedrzejewski, P. V. S. Marques, R. Romero, D. J. Webb, and I. Bennion, "Spectral characteristics of tapered LPG device as a sensing element for refractive index and temperature," *J. Lightwave Technol.* **24**(2), 870–878 (2006).
14. J. Villatoro and D. Monzón-Hernández, "Fast detection of hydrogen with nano fiber tapers coated with ultra thin palladium layers," *Opt. Express* **13**(13), 5087–5092 (2005).
15. K. P. Nayak, F. L. Kien, M. Morinaga, and K. Hakuta, "Antibunching and bunching of photons in resonance fluorescence from a few atoms into guided modes of an optical nanofiber," *Phys. Rev. A* **79**(2), 021801 (2009).
16. V. G. Minogin and S. N. Chormaic, "Manifestation of the van der Waals surface interaction in the spontaneous emission of atoms into an optical nanofiber," *Laser Phys.* **20**(1), 32–37 (2010).
17. E. Vetsch, D. Reitz, G. Sagué, R. Schmidt, S. T. Dawkins, and A. Rauschenbeutel, "Optical interface created by laser-cooled atoms trapped in the evanescent field surrounding an optical nanofiber," *Phys. Rev. Lett.* **104**(20), 203603 (2010).
18. S. Weis, R. Rivière, S. Deléglise, E. Gavartin, O. Arcizet, A. Schliesser, and T. J. Kippenberg, "Optomechanically induced transparency," *Science* **330**(6010), 1520–1523 (2010).
19. J. M. Ward, Y. Wu, V. G. Minogin, and S. N. Chormaic, "Trapping of a microsphere pendulum resonator in an optical potential," *Phys. Rev. A* **79**(5), 053839 (2009).
20. B. Misra and E. C. G. Sudarshan, "The Zeno's paradox in quantum theory," *J. Math. Phys.* **18**(4), 756–763 (1977).
21. W. M. Itano, D. J. Heinzen, J. J. Bollinger, and D. J. Wineland, "Quantum Zeno effect," *Phys. Rev. A* **41**(5), 2295–2300 (1990).
22. Y. Huang, J. B. Altepeter, and P. Kumar, "Interaction-free all-optical switching via the quantum Zeno effect," *Phys. Rev. A* **82**(6), 063826 (2010).
23. H. Sasada, "Wavenumber measurements of sub-Doppler spectral lines of Rb at 1.3 pm and 1.5 pm," *IEEE Photon. Technol. Lett.* **4**(11), 1307–1309 (1992).
24. H. S. Moon, W. K. Lee, L. Lee, and J. B. Kim, "Double resonance optical pumping spectrum and its application for frequency stabilization of a laser diode," *Appl. Phys. Lett.* **85**(18), 3965–3967 (2004).
25. J. E. Bjorkholm and P. F. Liao, "Line shape and strength of two-photon absorption in an atomic vapor with a resonant or nearly resonant intermediate state," *Phys. Rev. A* **14**(2), 751–760 (1976).
26. B. V. Zhdanov and R. J. Knize, "Progress in alkali lasers development," *Proc. SPIE* **6874**, 68740F, 68740F-12 (2008) (and references therein).

1. Introduction

All-optical modulation and switching are important for optical communication and quantum information processing [1–5]. Conventional techniques of non-linear optics typically require relatively high power, and are not well suited for these applications. An ultra-low power quantum Zeno effect based optical modulator using a degenerate V-system and a tapered nano fiber embedded in Rb vapor has recently been demonstrated by us [6]. Unfortunately, this is not useful for switching optical fields in the telecommunication band. On the other hand, the ladder type Zeno modulator described here can be used to modulate signals at 1323 nm, using a control beam at 795 nm. In combination with a tapered nano fiber (TNF) setup [6–9], this modulator can be used to produce an optical modulator at extremely low powers of the control beam (~40nW). The TNF-based modulator could also be integrated with other applications of TNF such as super-continuum generation [10], coupling light into microsphere resonators [11,12], near-field sensing [13,14], investigation of interaction of evanescent field with cold atoms [15–17], and exploration of opto-mechanical effects [18,19].

2. The quantum Zeno effect in a ladder transition

The quantum Zeno effect (QZE) [20–22] refers in general to the suppressed evolution of a quantum state through the quantum measurement process. However, in all instances, the QZE can be interpreted more transparently in terms of AC-Stark shifts or splitting, without invoking the concept of measurement explicitly [6]. Using this approach, the basic mechanism of the degenerate V-system Zeno switch has been explained in terms of the QZE [6]. Specifically, in [6], the QZE was shown to be a manifestation of the AC-Stark splitting of dressed states. A similar interpretation also holds when a three level system involving a

ladder type transition is used. As shown in Fig. 1(a), the system consists of three states: a ground state ($|1\rangle$), a strongly-damped intermediate state ($|2\rangle$), and a third state ($|3\rangle$) which may or may not be strongly damped. The control beam couples $|1\rangle$ to $|2\rangle$, and the probe beam couples $|2\rangle$ to $|3\rangle$. For resonant excitation, the corresponding dressed states (defined as products of photon number states and atomic states) are degenerate, as shown in Fig. 1(b). When the coupling between $|1\rangle$ and $|2\rangle$ is strong, the resulting states, upon diagonalization ($|+\rangle$ and $|-\rangle$) are split by an amount equaling the Rabi frequency of the $|1\rangle$ to $|2\rangle$ transition, which is much larger than the natural linewidth of $|2\rangle$, as illustrated in Fig. 1(c).

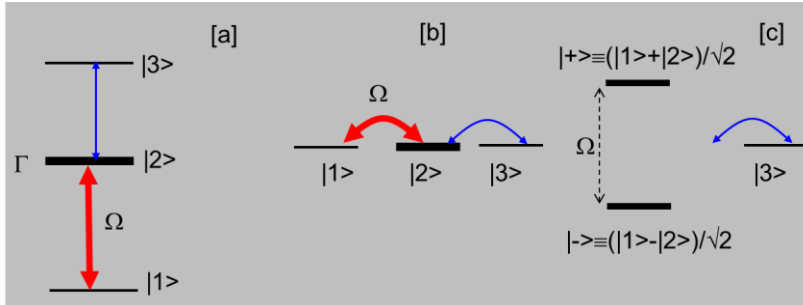


Fig. 1. AC-Stark effect in a Ladder Transition: (a) The control beam couples $|1\rangle$ to $|2\rangle$, and the probe beam couples $|2\rangle$ to $|3\rangle$; (b) For resonant excitation, the corresponding dressed states are degenerate; (c) When the strong control beam coupling is diagonalized, the resulting states are split by an amount much larger than the natural linewidth of $|2\rangle$.

There are several combinations of parameters that can be considered for controlling the probe absorption. Consider first Case I, where the probe is resonant for the $|2\rangle$ to $|3\rangle$ transition, but the pump is relatively weak, so that the two diagonalized states ($|+\rangle$ and $|-\rangle$) are not resolved. In this case, the probe is transparent when the pump is not present (since the atoms remain in state $|1\rangle$), and is absorbed when the pump is turned on. Consider next Case II where the pump is strong so that the two diagonalized states are clearly resolved, but the probe is detuned from the $|2\rangle$ to $|3\rangle$ transition (positively or negatively) by half the separation between the two diagonalized states. In this case, the probe is absorbed in the presence of the pump, but is transparent when the pump is not present. This is the same as what happens for Case I, but for different reasons. Finally, consider Case III, where again the pump is strong so that the two diagonalized states are clearly resolved, but the probe is resonant for the $|2\rangle$ to $|3\rangle$ transition (as shown in Fig. 1). In this case, the probe is transparent both in the presence and in the absence of the pump. Cases I and II can be considered to be QZE-based control of probe absorption, since the mechanism in each case can be interpreted in terms of AC-Stark effects. In this paper, we describe experimental results based on Case I, while the scheme we describe for high speed modulation in the presence of buffer gas is based on Case II.

3. Experimental set-up

In this section, we describe our experiment for realizing a Case I type QZE modulator in a conventional vapor cell of length ~ 7.5 cm, under free space propagation of light. The experimental configuration is illustrated schematically in Fig. 2. Briefly, beams from two tunable lasers (a Ti-Sapphire laser at 795 nm, and a fiber laser at 1323 nm) are combined with a dichroic mirror (DCM). Both the control and the signal beams are co-propagating, and linearly polarized in the same direction. A part of the 795 light is sent to a reference vapor cell for saturated absorption spectroscopy and locking. The combined beams are sent through a vapor cell, shielded from magnetic fields with μ -metal. After passing through the cell, another DCM is used to split the light into two parts, and the signal at each frequency is monitored with a separate detector. The cell is heated to temperatures of about 150° C using bifilarly wound wires that do not add any magnetic fields. For ^{85}Rb we estimated

experimentally the optical depth for the strongest transition ($5S_{1/2}, F = 3, m_F = 3$ to $5P_{3/2}, F = 4, m_F = 4$) on the D2 line to be ~ 220 , corresponding to an atomic density of $\sim 10^{10} \text{ cm}^{-3}$. For ^{87}Rb the optical density for the strongest transition ($5S_{1/2}, F = 2, m_F = 2$ to $5P_{3/2}, F = 3, m_F = 3$) on the D2 line was estimated to be ~ 85 , corresponding to an atomic density of $\sim 3.8 \times 10^9 \text{ cm}^{-3}$.

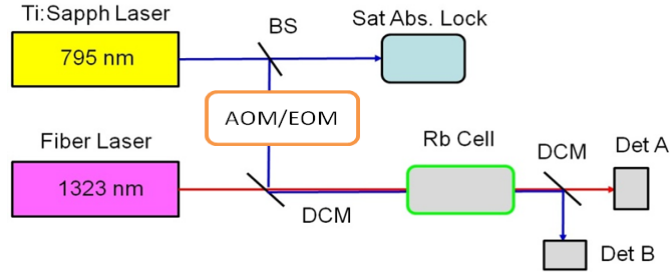


Fig. 2. Schematic illustration of the experimental setup for observing the ladder-transition based QZE modulator. DCM: Dichroic mirror, AOM: Acousto-Optic modulator, EOM: Electro-Optic modulator, BS: Beam Splitter

The acousto-optic modulator (AOM) and the electro-optic modulator (EOM) shown in Fig. 2 are used only while performing the actual modulation, and are removed while characterizing the absorption profile at 1323nm. While performing spectroscopic measurements and switching at low frequencies (up to $\sim 5\text{MHz}$), we used Thorlabs PDA55 (Silicon) and Thorlabs PDA400 (InGaAs) for detecting light at 795nm and 1323nm respectively. For high frequency switching, a fast APD (New Focus 1647) with a bandwidth of 1 GHz was used for detection of 1323nm light.

4. Spectroscopic details

We chose to use the $5S_{1/2} \rightarrow 5P_{1/2} \rightarrow 6S_{1/2}$ ladder transition in Rb for our experiment, dictated in part by lasers readily available to us. Using the reference saturated absorption cell, we locked the pump laser (795 nm) to one of the resonances of the $5S_{1/2} \rightarrow 5P_{1/2}$ manifold and the probe laser (at 1323nm) was then scanned across the $6S_{1/2}$ manifold over a few GHz. The modulator should work just as well if the ladder transition is of the type $5S_{1/2} \rightarrow X \rightarrow Y$, where X is $5P_{1/2}$ or $5P_{3/2}$, and Y can be one of many states that are coupled to the X states via optical dipole transitions and have higher energies than that of X. For example Y can be $7S_{1/2}$, $4D_{3/2}$, $4D_{5/2}$, $5D_{3/2}$, $5D_{5/2}$, and so on.

Figure 3(a) shows the spectroscopic details of the ladder transition for ^{85}Rb . The probe beam was scanned over the $6S_{1/2}$ manifold while the control beam was locked to the $F = 2 \rightarrow F = 2$ transition on the lower leg. The separation between the hyperfine levels in the $5P_{1/2}$ manifold ($\sim 360 \text{ MHz}$) is less than the Doppler linewidth ($\sim 600 \text{ MHz}$). Hence, atoms are excited to both hyperfine levels of the $5P_{1/2}$ manifold even if the 795nm laser is locked to only the $F = 2 \rightarrow F = 2$ transition. As a result, it is expected that 4 lines would be observed for the 1323nm absorption (upper leg) as this laser is scanned over a few GHz (Fig. 3(b)). However, it is to be noted that, due to Doppler shift, the atoms excited to the $F = 3$ state of the intermediate level correspond to negative velocity (with respect to the direction of propagation of the 795 nm laser beam) atoms, and not zero velocity atoms. Thus, the transitions from this state to the $6S_{1/2}$ manifold are shifted to lower frequencies by an amount equal to the separation between the hyperfine states in the $5P_{1/2}$ manifold ($\sim 360 \text{ MHz}$). In the case of ^{85}Rb , the frequency difference between the hyperfine states in the $6S_{1/2}$ manifold ($\sim 710 \text{ MHz}$) is such that this shift causes the $F = 2 \rightarrow F = 2$ transition almost to overlap the $F = 3 \rightarrow F = 3$ transition, for the 1323 nm beam. As a result, only 3 lines are expected to be observed distinctly (see Fig. 3(c)). It is to be noted that Figs. 3(b) and 3(c) only illustrate the

expected relative positions of the ^{85}Rb absorption lines (at 1323nm), and not the actual observed data, which are described next.

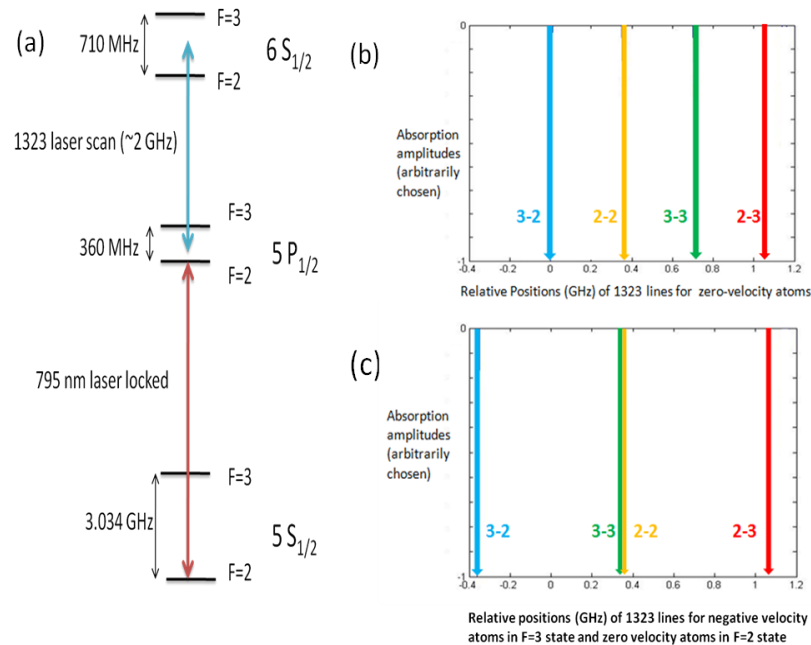


Fig. 3. Spectroscopic details of ladder transition in ^{85}Rb (a) Schematic of various hyperfine levels used, along with the transition frequencies. (b) Expected spectrum if both hyperfine states of intermediate level are occupied by zero velocity atoms. (c) Shift of spectrum in (b) due to $F = 3$ state at the intermediate level being occupied by negative velocity atoms

Figures 4(a) and 4(b) show a couple of typical profiles that were observed for ^{85}Rb . The data in Fig. 4(a) corresponds to a relatively low power (~ 2 mW) of the control beam, and only three absorption lines are observed, in keeping with the explanation provided in Fig. 3 above. The relative separation between the lines is in good agreement with the expected spectrum, as illustrated in Fig. 3(c). This data has been taken in AC mode (on a standard digital oscilloscope) and hence shows negative values. The slow background modulation seen in the signal is most likely due to the etalon effect from the windows of the cell. The data in Fig. 4(b), taken in DC mode, corresponds to much higher power (~ 200 mW) of the control beam, and we see almost complete absorption of the probe while the lines are strongly power broadened. Of course, the amount of 1323nm absorption increases with the number of atoms excited to the intermediate leg, which in turn is determined by the power of the control beam. Thus at sufficiently high power of the control beam, the upper transition is completely saturated. It should be noted that even in this case, the pump power is not high enough to correspond to Case II, since the power broadening is less than the effective width of the intermediate state (~ 600 MHz) due to Doppler broadening.

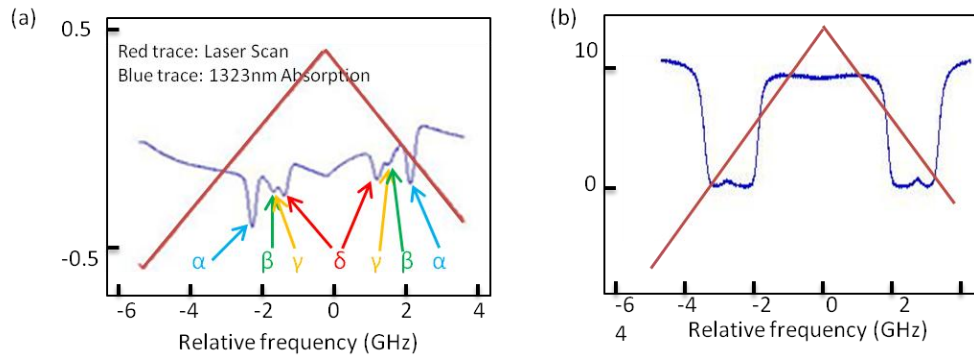


Fig. 4. Typical absorption profiles for the ladder transitions (at 1323nm) that are observed in ^{85}Rb . (a) Corresponds to 795 nm laser power $\sim 2\text{mW}$, data taken in AC mode; the hyperfine transitions corresponding to the absorption dips are α : $3 \rightarrow 2$, β : $3 \rightarrow 3$, γ : $2 \rightarrow 2$, δ : $2 \rightarrow 3$. Note that the spectrum is seen in the reverse order during the repeat scan. (b) Corresponds to 795 nm laser power $\sim 200\text{mW}$; we see near 100% absorption and the lines are highly power broadened. The null value of the probe detuning is defined arbitrarily to be at the turn-around point of the scan in each case.

Figure 5 shows the spectroscopic details for ^{87}Rb and a few typical absorption profiles that were observed at 1323nm. The control laser was locked to the $F = 1 \rightarrow F = 1$ transition on the lower leg, as shown in Fig. 5(a). For moderately high powers ($\sim 50\text{mW}$) of the control beam, atoms get excited to both hyperfine levels of the $5P_{1/2}$ manifold, due to power broadening of the $5S_{1/2} \rightarrow 5P_{1/2}$ transition. At these powers, we can clearly resolve 4 absorption lines, as shown in Fig. 5(b). It is worth noting that each of the lines is control-power-broadened because of the fact that a significant number of velocity groups are excited to both hyperfine states of the intermediate level due to the relatively high power of the control beam. At sufficiently low powers of the control beam ($\sim 0.5\text{mW}$), two of the four lines are almost completely suppressed, and each individual line can be seen as a narrow sharp line, as illustrated in Fig. 5(c).

As before, the data in Fig. 5(b) and Fig. 5(c) have been taken in AC mode on a standard digital oscilloscope, and hence show negative values. The slow background modulation observed in both figures is again most likely due to the etalon effect of the Rb cell window, as mentioned previously.

It should be noted that ladder transitions of this type have been studied previously, theoretically as well as experimentally [23–25], in different contexts. The Doppler-free nature of the upper leg of the ladder transition in the co-propagating configuration is consistent with the theoretical model presented in [25], and the experimental results presented in [24,25]. The hyperfine splitting frequencies we have observed for the $5P_{1/2}$ to $6S_{1/2}$ transition for both ^{85}Rb and ^{87}Rb are in agreement with those reported in [23]. However, the experiment reported in [23] did not show any absorption lines for this transition; therefore, a quantitative comparison of the spectral response is not possible. Finally, the accidental near-degeneracy we have observed between the $F = 3 \leftrightarrow F = 2$ and $F = 2 \leftrightarrow F = 2$ transitions on the upper leg in the case of ^{85}Rb due to contributions from different velocity groups (as illustrated in Fig. 3(c) and Fig. 4(a)) has not been reported in any of these references.

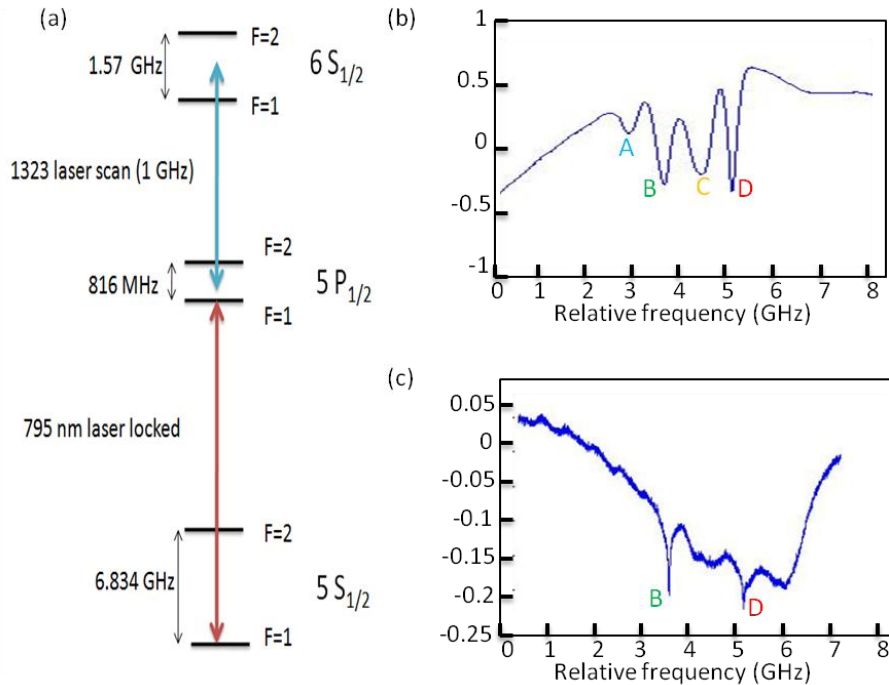


Fig. 5. Spectroscopic details of ladder transition in ^{87}Rb (a) Schematic of various hyperfine levels used along with the transition frequencies. (b) Absorption corresponding to 795 nm laser power $\sim 50\text{mW}$; all four transitions can be clearly seen. The hyperfine transitions corresponding to the absorption dips are A: $2 \rightarrow 1$, B: $1 \rightarrow 1$, C: $2 \rightarrow 2$, D: $1 \rightarrow 2$. (c) Corresponds to 795 nm laser power $\sim 0.5\text{mW}$; two of the four lines are suppressed and only transitions from $F = 1$ are observed.

5. Modulation

In order to demonstrate modulation, we chose to use the strongest absorption line at the upper leg of transitions, which in our case was the $F = 3 \rightarrow F = 2$ resonance for ^{85}Rb (due in part to the fact that in a natural mixture of Rb, 72.15% is ^{85}Rb , and 27.85% is ^{87}Rb). Keeping the probe laser (1323 nm) parked on this resonance, we then modulated the amplitude of the pump beam (795 nm). At low frequencies, switching of the control beam was accomplished using an AOM while for higher frequencies, an EOM configured for intensity modulation was used. The result is shown in Fig. 6.

For low frequencies, we used a pump power of $\sim 200\text{mW}$ and we see a strong modulation, in phase with the pump modulation, with a modulation depth of essentially 100% up to a speed of 1MHz. The modulation depths obtained while using the EOM were smaller because of the low control beam power ($\sim 2\text{mW}$) used. This was necessitated by the damage threshold ($\sim 20\text{mW}$) of the EOM used to switch the pump beam and the relatively low efficiency of the EOM ($\sim 20\%$). We have tested the modulation up to a speed of 75 MHz, and determined a 3dB bandwidth of approximately 5 MHz, as shown in Fig. 7. In Fig. 7, we have plotted the modulation amplitude at various frequencies (obtained using the EOM), normalized to the amplitude at 1MHz, where the modulation depth was essentially 100%, when obtained with the AOM.

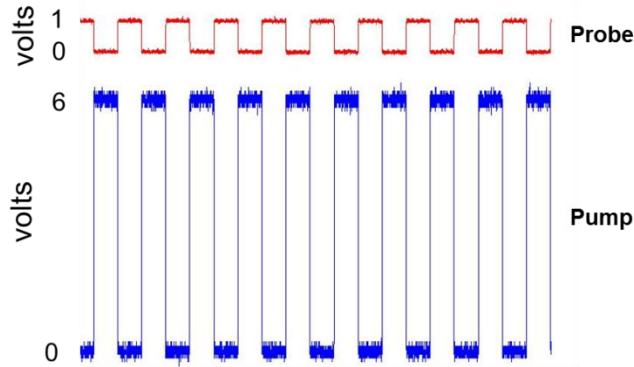


Fig. 6. Voltage as measured by the probe and pump detectors (top and bottom respectively) at a frequency of ~ 1 MHz. The intensities are directly proportional to the voltages recorded.

A careful consideration of the physical mechanism behind this modulation reveals that the modulation speed is fundamentally limited by the time needed for the atoms to repopulate the ground state, after the pump is turned off, so that they can absorb the probe again. This means that the modulation bandwidth cannot exceed the homogeneous linewidth (HL). This constraint is rather obvious for Case I, which has been employed here. As we will discuss later, this constraint on the maximum speed also holds if Case II is employed for modulation.

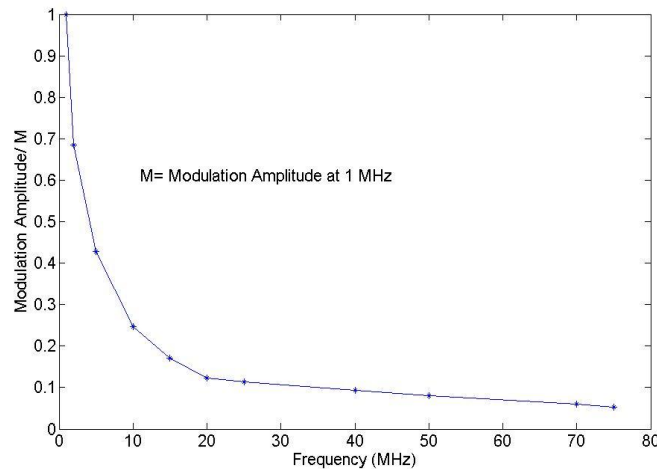


Fig. 7. Modulation amplitude (normalized to the amplitude at 1 MHz) vs. frequency

6. High speed modulation – proposed experiment and simulation results

6.1 Proposed experiment

The HL can be increased very significantly by adding a buffer gas, such as ^4He . In a series of studies carried out in the context of the development of diode pumped alkali lasers (DPALs) [26], it has been shown that the atoms excited to the $5P_{3/2}$ state relaxes very rapidly to the $5P_{1/2}$ state.

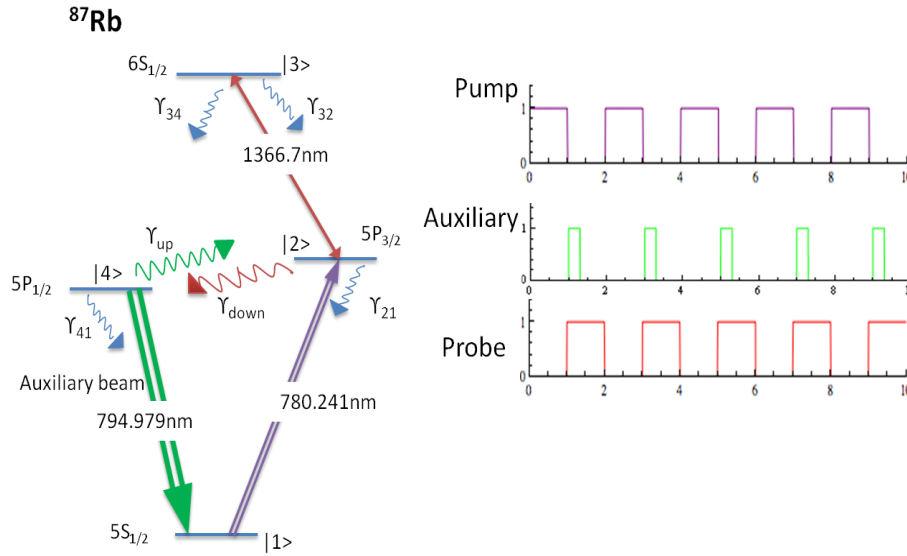


Fig. 8. Schematic of modulator in the presence of buffer gas and auxiliary beam. The reciprocal relaxation rates (γ_{down} and γ_{up}) for the $5P_{1/2}$ and $5P_{3/2}$ states can be controlled by the pressure of the buffer gas. Typically, $\gamma_{\text{up}} \approx \gamma_{\text{down}} / 4$. For a pressure of about 1 atm, $\gamma_{\text{down}} \approx 10$ GHz. The γ_{mn} (m and n integers) relaxation rates along the optical transitions are due to radiative decays, and are not affected by the buffer gas. Specifically, $\gamma_{34} = \gamma_{32} \approx 3$ MHz and $\gamma_{21} = \gamma_{41} \approx 6$ MHz. A schematic of the timing sequence of the pump and the auxiliary beam and the expected probe absorption are shown on the right.

This process increases the HL for the pump transition significantly. For example, HL (given effectively by γ_{down} , which is much larger than γ_{21}) is about 10 GHz for a buffer gas pressure of 1 atm, and can be as large as 500 GHz for a pressure of 25 atm. However, the rate of decay from the $5P_{1/2}$ state to the ground state is not affected by the presence of the buffer gas, thus preventing rapid repopulation of the ground state. This effect would normally limit the maximum modulation speed achievable. But, this constraint can be circumvented via the addition of an auxiliary beam (which we henceforth call the deshelving beam) that would be turned on at the same time as the pump is turned off, and turned off before turning on the pump again, as illustrated in Fig. 8. For best performance, (in terms of contrast obtained during modulation) the pulse width of the de-shelving beam applied should be much smaller than the time scale of the dominant relaxation rate (namely $1/\gamma_{\text{up}}$) from the $5P_{1/2}$ state. However, even for longer pulse widths (up to $100/\gamma_{\text{up}}$), the system produces very good contrast. Furthermore, this beam should be as close as possible to an ideal π -pulse in a 2-level system. The de-shelving beam causes rapid repopulation of the ground state, thereby ensuring atoms can be cycled back to the $5P_{3/2}$ state when the pump is turned on again. The speed would be limited by the dominant relaxation rate (γ_{down}) of the $5P_{3/2}$ state, which is in turn controlled by the buffer gas pressure. It is to be noted that while we have chosen to use $6S_{1/2}$ as the highest level to illustrate this scheme, there are many other states (e.g., $7S_{1/2}$, $4D_{3/2}$, $4D_{5/2}$, $5D_{3/2}$, $5D_{5/2}$ and so on) that would work just as well. However, for optimal operation, the intermediate state must be $5P_{3/2}$, since the quenching rate is higher from $5P_{3/2}$ to $5P_{1/2}$ than that in the reverse direction.

6.2 Simulation results

Preliminary results obtained from the simulation of the system shown in Fig. 8 are presented in Fig. 9. The values of the decay rates used were $\gamma_{\text{down}} \sim 10$ GHz, $\gamma_{\text{up}} \sim 2.5$ GHz, $\gamma_{34} = \gamma_{32} \sim 3$

MHz and $\gamma_{21} = \gamma_{41} \sim 6$ MHz. The simulations are carried out using the Case II configuration, with the negative probe detuning matched to half the Rabi frequency. Thus, the probe is resonant with the $|+\rangle \rightarrow |3\rangle$ transition. The residual oscillations seen in the probe absorption occur at the pump Rabi frequency.

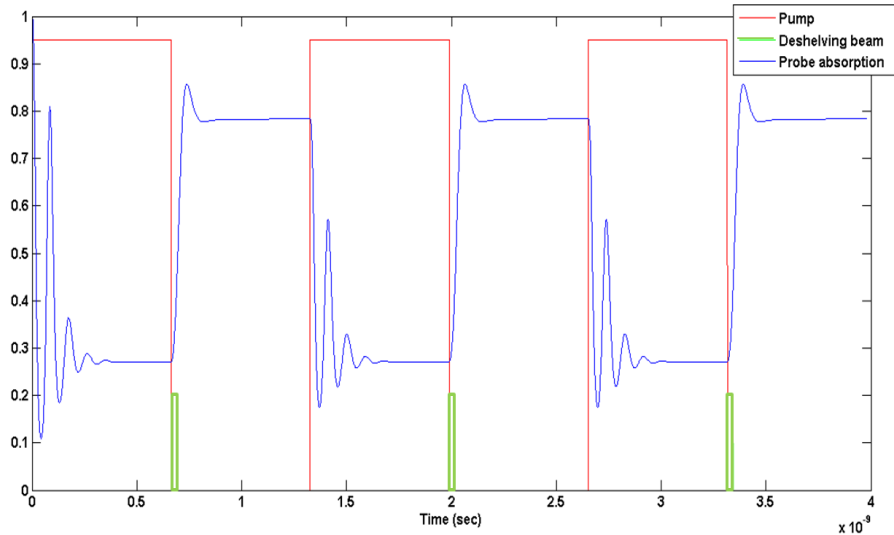


Fig. 9. High speed modulation in the presence of buffer gas, and using an auxiliary (deshelving) beam. The power levels of the pump and the deshelving beam have been rescaled. The deshelving beam is applied immediately after turning off the pump and for a very short duration. The modulation speed is about 1 GHz. The temporal width of the deshelving π -pulse used for the simulation is $2/\gamma_{\text{down}}$.

These oscillations can be understood clearly by considering the limiting case where state $|2\rangle$ is completely undamped ($\gamma_{\text{down}} = 0$, $\gamma_{21} = 0$), state $|3\rangle$ decays to state $|2\rangle$ only, and the deshelving beam is turned off, so that state $|4\rangle$ is completely decoupled from the system. In this case, the population of level $|2\rangle$ oscillates between 0 and 1 (in the limit of a vanishingly weak probe beam) at the rate of the pump Rabi frequency. Thus, if the configuration of Case I is employed, the probe absorption would obviously oscillate (between the maximum value and zero) at the same frequency. Oscillation of the probe absorption between the maximum value and zero also occurs if Case II is employed. The latter may appear to be somewhat surprising, since the population of the $|+\rangle$ level (as well as that of the $|-\rangle$ level) remains constant at a value of $1/2$, and the probe is resonant with $|+\rangle \rightarrow |3\rangle$ transition. On the other hand, it is sensible if one considers the fact that at some point in time there are no atoms in state $|2\rangle$. These two observations can be reconciled by noting that even though the probe is resonant with the $|+\rangle \rightarrow |3\rangle$ transition, there is also the off-resonant transition between the $|-\rangle$ state and state $|3\rangle$. For the very short time scale of the Rabi oscillation, the $|+\rangle$ and $|-\rangle$ state are effectively broadened by the Rabi frequency (akin to transit time broadening), in a manner so that during one point in the Rabi oscillation cycle, the imaginary part of ρ_{32} , which determines the probe absorption (ρ being the density matrix) vanishes due to equal and opposite contributions from the $|+\rangle$ and $|-\rangle$ states. We have verified this explicitly, using numerical simulations under this condition.

In the presence of the strong damping of level $|2\rangle$, as employed in the simulation for Fig. 9, these oscillations get damped, producing a steady-state absorption of the probe, on a time scale given by the damping rate of level $|2\rangle$. Thus, if we used the same technique, but without the buffer gas, the probe absorption would remain oscillatory through the whole time during which the pump is on, since the timescale for reaching steady state would be given by the

inverse of the radiative decay rate (γ_{21}) of level 2 only, corresponding to more than 30 nanosecond, which is much longer than the modulation rate shown in Fig. 9. Thus, employing Case II by itself is not enough to achieve high speed modulation; the rapid decay rate of level $|2\rangle$ is essential.

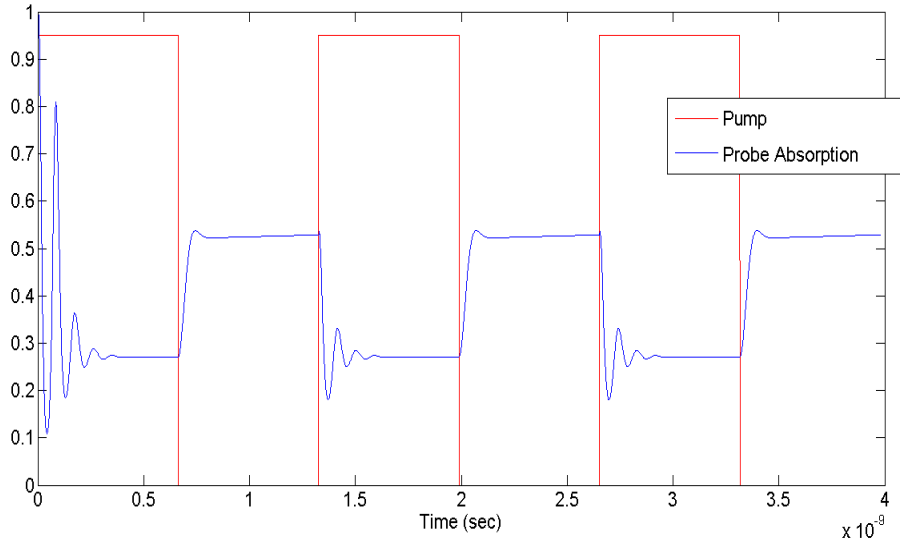


Fig. 10. High speed modulation using buffer gas but without any deshelving beam. The power level of the pump has been re-scaled. The switching speed is about 1 GHz.

In Fig. 10, we show results obtained for the same set of parameters as used in Fig. 9, except that the deshelving beam is not used. As can be seen, a modulation with a significant contrast is still achievable. Thus, the presence of the deshelving beam is not essential for obtaining high speed modulation. To see why this is the case, we recall from Fig. 8 that there is also a relaxation (γ_{up}) of atoms from the $5P_{1/2}$ state to the $5P_{3/2}$ state in the presence of buffer gas, at a rate which is about 4 times smaller than the decay rate (γ_{down}) in the opposite direction. Consequently, the atoms never leave the $5P_{3/2}$ state completely during the time when the pump is turned off. Half of these atoms get tuned back to resonance (between the $|+\rangle$ and $|3\rangle$ states) when the pump is turned back on, producing strong absorption. The reduced contrast in the absence of the deshelving beam is due to the fact that fewer number of atoms in state $|2\rangle$ decay to state $|4\rangle$ because there is no mechanism for atoms in state $|4\rangle$ to be transferred to state $|1\rangle$. In the presence of the deshelving beam, the number of atoms remaining in state $|2\rangle$ after the deshelving π -pulse is significantly smaller, thus producing higher transparency for the probe, and consequently higher modulation contrast.

For both cases (deshelving beam on or off), the modulation depth remains virtually uniform for increasing modulation speeds, but the rapid oscillations do not die off at higher speeds. In order to estimate the bandwidth of the modulator, we used the criterion that both the on and off states of the probe must reach a steady state value before the corresponding states of the pump. This gives a bandwidth of about 1.5 GHz for $\gamma_{down} = 10\text{GHz}$. The bandwidth can be increased further by increasing the value of γ_{down} (as well as $\gamma_{up} = \gamma_{down}/4$) and scaling the pump power by the same factor. Indeed, preliminary simulation results have shown that the bandwidth roughly scales with γ_{down} . More details about the impact of various parameters, such as pump and auxiliary beam powers, pulse-width of the de-shelving beam, and the decay rates, on the modulator performance in terms of modulation depth and bandwidth will be presented in a separate paper. Efforts are also underway in our laboratory to investigate the feasibility of realizing a buffer-gas augmented modulator of this type.

It should be possible to realize this scheme in a tapered nano fiber (TNF) set-up, yielding an efficient modulator at the telecom wavelength at very low control powers. The TNF will be designed to operate as a single mode fiber for all three wavelengths: 780 nm, 795 nm and 1323 nm. We have carried out designs of such a TNF, and have shown that there is a range of taper diameters for which it is possible to have a significant overlap between the evanescent modes at these three wavelengths. The TNF would be embedded in a Rb vapor cell, of the type reported in [7], and pressurized with a ^4He buffer gas at ~ 3 atm. The pump and the auxiliary beams will be orthogonally polarized, and combined with a polarizing beam splitter. The probe will be combined with these beams using a dichroic mirror. The combined beams will be launched into the TNF. Similar techniques will be used to separate the probe from the other beams at the output. Of course, the intensity needed to saturate a 500 GHz broadening would be too hard to realize in a TNF. However, based on a typical DPAL laser employing Rb, which requires a threshold pump intensity of about $15 \mu\text{W}/\mu\text{m}^2$, we estimate that a pump power of about $3 \mu\text{W}$ should be enough to achieve a few GHz modulation bandwidth in the TNF, which has a mode area of only $0.2 \mu\text{m}^2$.

7. Conclusion

We have demonstrated a high-efficiency optical modulator at ~ 1323 nm using the quantum Zeno effect in a ladder transition in a Rb vapor cell. We observe cross-modulation of the signal beam transmission as the control beam is intensity modulated. We obtain a 3dB bandwidth of approximately 5 MHz, which can be improved to a few GHz by using buffer gas to enhance the homogenous broadening. The bandwidth can be controlled by the relaxation rates between the $5P_{1/2}$ and $5P_{3/2}$ states, which in turn are controlled by the buffer gas pressure. It should be possible to realize this scheme in a tapered nano fiber set-up, yielding an efficient modulator at the telecom wavelength at very low control powers.

Acknowledgments

This work was supported in part by AFOSR Grant # FA9550-10-01-0228, and the DARPA ZOE program under Grant # W31P4Q-09-1-0014.